J|A|C|S ARTICLES

Published on Web 12/24/2008

Electron Transport and Recombination in Solid-State Dye Solar Cell with Spiro-OMeTAD as Hole Conductor

Francisco Fabregat-Santiago,*,† Juan Bisquert,*,† Le Cevey,‡ Peter Chen,‡ Mingkui Wang,‡ Shaik M. Zakeeruddin,‡ and Michael Grätzel*,‡

Photovoltaics and Optoelectronic Devices Group, Departament de Física, Universitat Jaume I, 12071 Castelló, Spain, and Laboratory for Photonics & Interfaces, École Polytechnique Féderal de Lausanne, Lausanne CH-1015, Switzerland

Received July 26, 2008; E-mail: fran.fabregat@fca.uji.es; bisquert@fca.uji.es; michael.graetzel@epfl.ch

Abstract: We show that electron transport mechanisms in TiO_2 solid-state dye-sensitized solar cells (SDSCs) with spiro-OMeTAD as hole conductor are similar to those of high-performance DSCs with liquid electrolytes and ionic liquids. Impedance spectroscopy provides the parameters for transport and recombination at different conditions of steady state in the dark. The recombination rate is much higher in the solid solar cell, this being a main limiting step to obtain high-efficiency SDSCs. Thus, the expected gain in photovoltage, due to a lower hole Fermi level, is prevented by recombination losses. Under low potentials the transport is limited by the electron transport in the TiO_2, but at high potentials spiro-OMeTAD transport resistance reduces the fill factor and hence the efficiency on high-current devices.

1. Introduction

Industrialization of dye solar cells (DSCs) has generated a strong interest in the development of solid-state devices (SDSCs) using this technology. One of the approaches to substitute the liquid electrolyte used in the original solar cells is the use of (2,2′,7,7′-tetrakis(*N*,*N*-di-*p*-methoxyphenylamine)-9,9′-spirobifluorene (spiro-OMeTAD) as hole conductor.[1] Although efficiencies above 3% have been reached by several groups on this device,[2−4] the improvement of these values is currently limited by the lack of a deeper knowledge of the main parameters influencing the photoelectric behavior.

Several reports have been presented for the clarification of the different physicochemical characteristics and limitations of spiro-OMeTAD SDSCs,[5−9] with some interesting results. However, there are some aspects that still remain unclear, such as the origin of the low diffusion length found in these cells.

In this work we study the electrical behavior of spiro-OMeTAD-based SDSCs by applying different bias potentials in the dark and analyzing their impedance response using previously developed models.[10−12] This approach is different than the more commonly used method of measuring the electrical properties at different illumination conditions, although both are similarly based on displacing the Fermi level in the solar cell by injecting charges into it.[6,9] By studying the variations in the absence of photogeneration, we have the advantage that the hole density in the spiro-OMeTAD is largely unmodified. Another advantage of this approach is the possibility to directly compare the results obtained in spiro-OMeTAD SDSC parameters with other DSC configurations that we have reported previously, namely, high-efficiency liquid electrolyte DSC[13] and robust ionic-liquid-based DSC.[14] In this way, mechanisms dominating the response of the spiro-OMeTAD SDSC are identified and the differences with the other DSCs are noted. Finally, the role of these mechanisms in the efficiency of the cell are described, and proposals are made to improve the performance of the cells. The same procedure may be used in the characterization of solid-state solar cells that use other hole conductors, such as polymers (polythiophenes, polyanilines, etc.)[15,16] or p-type inorganic semiconductors (CuI, CuSCN).[17]

† Universitat Jaume I.
‡ École Polytechnique Féderal de Lausanne.

(1) Bach, U.; Lupo, D.; Comte, P.; Moser, J. E.; Weissörtel, F.; Salbeck, J.; Spreitzer, H.; Grätzel, M. *Nature* **1998**, *395*, 583.
(2) Snaith, H. J.; Moule, A. J.; Klein, C.; Meerholz, K.; Friend, R. H.; Grätzel, M. *Nano Lett.* **2007**, *7*, 3372.
(3) Snaith, H. J.; Schmidt-Mende, L. *Adv. Mater.* **2007**, *19*, 3187.
(4) Karthikeyan, C. S.; Thelakkat, M. *Inorg. Chim. Acta* **2008**, *361*, 635.
(5) Kron, G.; Egerter, T.; Werner, J. H.; Rau, W. *J. Phys. Chem. B* **2003**, *107*, 3556.
(6) Snaith, H. J.; Schmidt-Mende, L.; Grätzel, M.; Chiesa, M. *Phys. Rev. B* **2006**, *74*, 045306.
(7) Snaith, H. J.; Grätzel, M. *Adv. Mater.* **2007**, *19*, 3643.
(8) Jennings, J. R.; Peter, L. M. *J. Phys. Chem. C* **2007**, *111*, 16100.
(9) Howie, W. H.; Claeyssens, F.; Miura, H.; Peter, L. M. *J. Am. Chem. Soc.* **2008**, *130*, 1367.
(10) Bisquert, J. *J. Phys. Chem. B* **2002**, *106*, 325.
(11) Bisquert, J.; Garcia-Belmonte, G.; Fabregat-Santiago, F.; Compte, A. *Electrochem. Commun.* **1999**, *1*, 429.
(12) Fabregat-Santiago, F.; Bisquert, J.; Palomares, E.; Durrant, J. R. *J. Appl. Phys.* **2006**, *100*, 034510.
(13) Wang, Q.; Ito, S.; Grätzel, M.; Fabregat-Santiago, F.; Mora-Seró, I.; Bisquert, J.; Bessho, T.; Imai, H. *J. Phys. Chem. B* **2006**, *110*, 19406.
(14) Fabregat-Santiago, F.; Bisquert, J.; Palomares, E.; Otero, L.; Kuang, D.; Zakeeruddin, S. M.; Grätzel, M. *J. Phys. Chem. C* **2007**, *111*, 6550.
(15) Saito, Y.; Azechi, T.; Kitamura, T.; Hasegawa, H.; Wada, Y.; Yanagida, S. *Coord. Chem. Rev.* **2004**, *248*, 1469.
(16) Smestad, G. P.; Spiekermann, S.; Kowalik, J.; Grant, C. D.; Schwartzberg, A. M.; Zhang, J.; Tolbert, L. M.; Moons, E. *Sol. Energy Mater. Sol. Cells* **2003**, *76*, 85.
(17) O'Regan, B.; Lenzmann, F.; Muis, R.; Wuenke, J. *Chem. Mater.* **2002**, *14*, 5023.

 10.1021/ja805850q CCC: $40.75

Table 1. Characteristics of DSCs Used in This Study

	sample IL7	L9	L10	L11	OMeTAD
n-TiO_2 layer (μm)	6.8	6.8	12	12	1.8
scatter layer (μm)	4	4	2	4	0
dye	K19	K19	N719	N719	Z907
electrolyte	Z325	Z380	Z300	Z300	solid
area (cm^2)	0.28	0.28	0.28	0.28	0.128
porosity (%)	68	68	68	68	68
V_{oc} (V)	0.71	0.76	0.80	0.86	0.86
J_{sc} (mA cm^{-2})	14.0	17.0	17.5	17.0	9.1
FF	0.71	0.72	0.73	0.76	0.51
efficiency (%)	7	9	10	11	4

2. Experimental Section

Complete DSC devices were prepared by coating a transparent conducting oxide (TCO, solar glass 4 mm thickness, 10 Ω/□, Nippon Sheet Glass) with a several micrometer thick layer of nanoporous TiO_2 (n-TiO_2) made from 20 nm colloids. A scattering layer made of 400 nm TiO_2 particles was then deposited on top. The thickness of each layer is indicated in Table 1. In the case of the SDSC, prior to depositing the nanoporous film, a 100 nm compact layer of TiO_2 was deposited by spray pyrolysis over the TCO to avoid recombination losses with the spiro-OMeTAD.

Different dyes and electrolytes were used as specified in Table 1:

K-19 dye, Ru-(4,4′-dicarboxylic acid-2,2′-bipyridine)(4,4′-bis(*p*-hexyloxystyryl)- 2,2′-bipyridine)$(NCS)_2$, coadsorbed with phenylproprionic acid (PPA) for samples L9 and IL7;

N719, *cis*-di(thiocyanato)-*N*,*N*′-bis(2,2′-bipyridyl-4-carboxylic acid-4′-tetrabutylammonium carboxylate)ruthenium(II), for samples L10 and L11; and

Z907, *cis*-di(thiocyanato)-(2,2′-bipyridyl-4,4′-dicarboxylic acid)(4,4′-dinonyl-2,2′-bipyridyl)ruthenium(II), coadsorbed with GBA for the solid-state solar cells.

The electrolytes used were labeled as follow:

Z380 for 0.5 M *N*-methylbenzimidazole, 0.12 M guanidinium thiocyanate, and 0.2 M iodine (I_2) in a mixture of 1-methyl-3-propylimidazolium iodide and 1-methyl-3-ethylimidazolium thiocyanate, 65%:35% volume ratio, used in IL7;

Z325 for 0.6 M methylpropylimidazolium iodide, 0.5 M *tert*-butylpyridine, and 0.03 M I_2 in a mixture of acetonitrile and valeronitrile, 75%:25% volume ratio, used in L9; and

Z300 for 0.60 M butylmethylimidazolium iodide, 0.03 M I_2, 0.10 M guanidinium thiocyanate, and 0.50 M 4-*tert*-butylpyridine in the mixture of acetonitrile and valeronitrile, 85%:15% volume ratio, used in L10 and L11.

For the liquid cells, the dye-adsorbed TiO_2 electrode and Pt-counter electrode were assembled into a sealed sandwich-type cell by heating with a hot-melt of ionomer film (Surlyn 1702, 25 μm thickness, DuPont) as a spacer between the electrodes. Electrolyte was introduced on the sandwich and sealed through a drilled hole in the counter electrode using a Bynel film (4702 from DuPont) and a thin cover glass.

In the case of SDSC, the spiro-OMeTAD (Covion) hole conductor was dissolved in chlorobenzene at a concentration of 170 mM together with 13 mM $Li[(CF_3SO_4)_2N]$ and 110 mM 4-*tert*-butylpyridine. The TiO_2 film was spin-coated for 30 s at 2000 rpm. After these operations, a gold electrode was deposited on top, and the cell formed was sealed with a top glass.

Characteristic performance parameters of the cells given in Table 1 were taken at 1 sun illumination, provided by a 1000 W xenon lamp filtered to AM 1.5 conditions and using a 0.16 cm^2 mask. Impedance data of SDSC under illumination were provided by a white light-emitting diode as light source at incident power of 10 mW cm^{-2}. The same light power was used to compare the resistances of different hole transporter media.

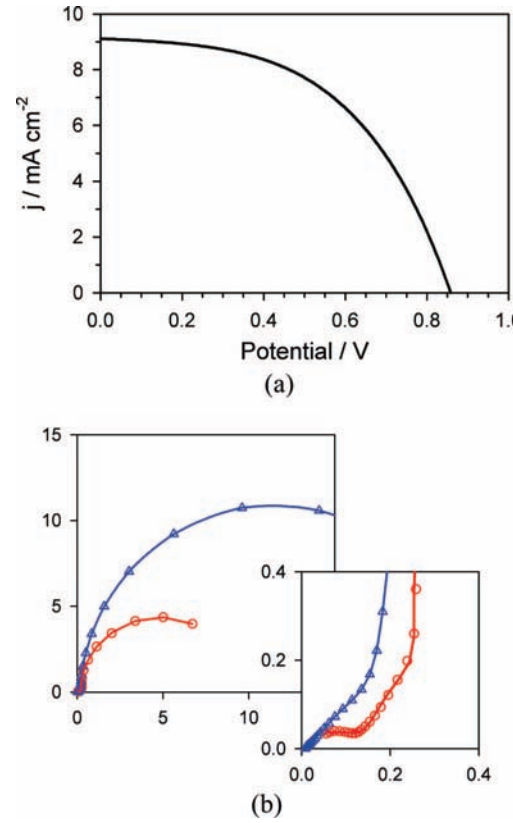

Figure 1. (a) $j-V$ curve of a SDSC measured under 1 sun conditions in a solar simulator. (b) Impedance spectra of SDSC (red circles) under low illumination conditions at 0.5 V and DSC, sample L10 (blue triangles), at 0.35 V. In these conditions both cells present similar TiO_2 transport resistance. Dots represent experimental data, and lines the fit to a transmission line model.

The impedance spectra were obtained using a PGSTAT-30 potentiostat from Autolab equipped with an impendance module. Data obtained were fitted using a two-channel model described elsewhere.[11,12]

3. Results and Discussion

The characteristic current density vs potential ($j-V$) curve and impedance spectra of a fresh SDSC in the dark are shown in Figure 1. The $j-V$ curve (Figure 1a) presents a low fill factor and low photocurrent due to the small thickness of the absorbing layer. The origin of these limitations to energy conversion efficiency will be discussed in more detail below.

In Figure 1b, the impedance spectrum of the SDSC is compared with the typical spectrum of a high-performance (10% efficiency) liquid electrolyte DSC at potentials in which both present similar transport resistances for electrons in TiO_2. In these conditions we observe that recombination resistance is much larger for the DSC than for the SDSC. The inset shows an additional arc at high frequencies in the SDSC. In liquid DSCs this arc is much smaller and behaves in a different way as a function of potential.

These spectra follow well a transmission line behavior according to the models in Figure 2. The transmission line model shown in Figure 2a, with resistance in a single channel corresponding to electron transport in TiO_2 nanostructure, has been applied on DSC in several works.[13,14] The fact that spiro-OMeTAD presents a higher transport resistance than liquid electrolytes makes the model more complex, and it is necessary to introduce an additional resistance in the (lower) channel

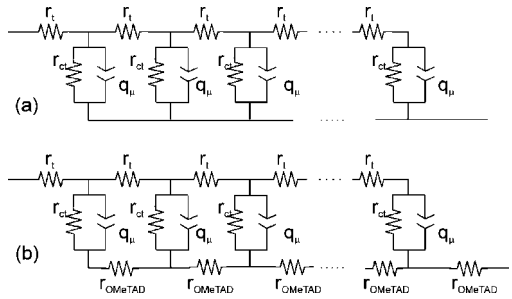

Figure 2. Two-channel transmission line model used to fit the impedance data of DSC (a) and SDSC (b). r_t represents the transport resistance in TiO_2, r_{ct} the interfacial charge-transfer resistance (or recombination resistance) between electron and hole carrier media, q_μ the chemical capacitance of TiO_2, and r_{OMeTAD} the resistance of the spiro-OMeTAD. For the fit of experimental data, it is necessary to add to this transmission line model a series resistance and a parallel capacitance in order to account for TCO resistance and underlayer/OMeTAD interfacial capacitance, respectively.

describing transport in the hole conductor.[11,12] Therefore, the model used was the two-channel resistance transmission line shown in Figure 2b. This new resistance in the model, coupled with the parallel capacitances for TCO/underlayer/OMeTAD interfacial capacitance, is responsible for the appearance of a high-frequency arc.

We have considered that the Fermi level in spiro-OMeTAD is stationary. From the fitting to two-channel transmission line models, we obtain the characteristic elements that describe the electronic processes occurring in the cell. The main elements that have been analyzed are electron transport resistance, R_t, and electron chemical capacitance, C_μ, in TiO_2, transport resistance in spiro-OMeTAD, R_{OMeTAD} and finally, recombination resistance, R_{ct}, at the interface between the electron and hole transport media.

From R_t and using the geometrical parameters given in Table 1, we determine the conductivity of electrons in the nanostructured TiO_2. It has been established that this conductivity is exclusively dependent on the number of free electrons in extended states, $\sigma = e\mu n$ (e is the elementary charge and μ the mobility),[13,18] and thus it provides a reasonable reference of the position of the Fermi level of the electrons (E_{Fn}) with respect to the conduction band edge (E_{cb}) as

$$\sigma = \sigma_0 \exp\left[\frac{E_{Fn} - E_{cb}}{k_B T}\right] \quad (1)$$

σ_0 being a constant, k_B the Boltzmann constant, and T the temperature. It must be furthermore emphasized that, in a multiple trapping scheme, the electron conductivity is independent of the number of traps. This is because σ relates only to the steady-state transport and reflects the rate of displacement in the transport band. In contrast to this, the chemical diffusion coefficient depends heavily on the occupation of traps. These points have been amply discussed in a recent paper.[19] According to this understanding, the conductivity is determined by the difference between E_{Fn} and E_{cb}, and thus we take the electron conductivity as a reference of such difference that will allow us to compare the properties of different kinds of DSCs at the same electronic state. In this way we compensate for the different shifts of the conduction band that are known to occur

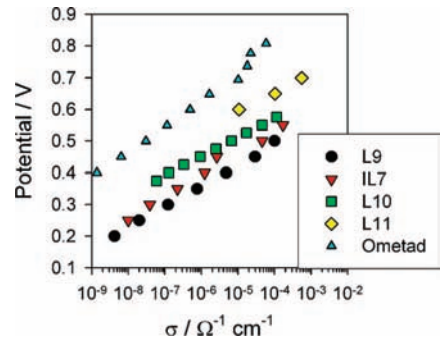

Figure 3. Potential in several DSCs as a function of the conductivity obtained from impedance spectroscopy.

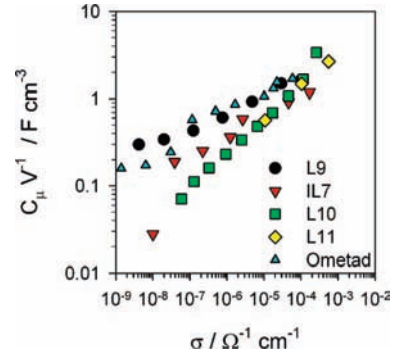

Figure 4. Chemical capacitance (per unit volume) in several DSCs as a function of electron conductivity.

when changing the medium and/or additives that fill the pores in a DSC.

Taking into account that the potential, applied or measured in the solar cell, is the difference between the E_{Fn} and the Fermi level of holes, E_{Fp}, in the hole conducting media (i.e., redox potential of I^-/I_3^- in liquid cells, and Fermi level of holes in OMeTAD), a comparison of the potentials in cells vs conductivity informs us about the distance between the conduction band and E_{Fp} (Figure 3). A remarkable increase of the potential is obtained in the SDSC with respect to other DSCs, which is attributed to the lower position of the spiro-OMeTAD Fermi level[20] than that of the redox potential of I^-/I_3^-, rather than high conduction band shifts which eventually would lead to a decline in the injection capacity of the dye.[21,22] We remark that the large energy difference between the Fermi level of holes in spiro-OMeTAD and TiO_2 conduction bands offers the prospect of a consequently larger photovoltage, with respect to the liquid cells, and this will be further discussed below.

If we represent the other parameters of the impedance results referred to TiO_2, i.e., C_μ and R_{ct} (normalized to remove the difference due to physical dimensions of the separate solar cells), versus the conductivity, we may compare the properties of the different DSC configurations when the conduction band is filled with the same amount of electrons (i.e., $E_{Fn} - E_{cb} =$ constant). This is shown in Figures 4−7. In the case of R_{ct} for samples with the same porosity and colloidal size (which is the case in the samples used here), the volume of the film is proportional to its effective internal surface.

(18) Abayev, I.; Zaban, A.; Fabregat-Santiago, F.; Bisquert, J. *Phys. Status Solidi (a)* **2003**, *196*, R4.
(19) Bisquert, J. *Phys. Chem. Chem. Phys.* **2008**, *10*, 3175.
(20) García-Cañadas, J.; Fabregat-Santiago, F.; Bolink, H.; Palomares, E.; Garcia-Belmonte, G.; Bisquert, J. *Synth. Met.* **2006**, *156*, 944.
(21) Hagfeldt, A.; Björkstén, U.; Grätzel, M. *J. Phys. Chem.* **1996**, *100*, 8045.
(22) Fabregat-Santiago, F.; Bisquert, J.; Garcia-Belmonte, G.; Boschloo, G.; Hagfeldt, A. *Sol. Energy Mater. Sol. Cells* **2005**, *87*, 117.

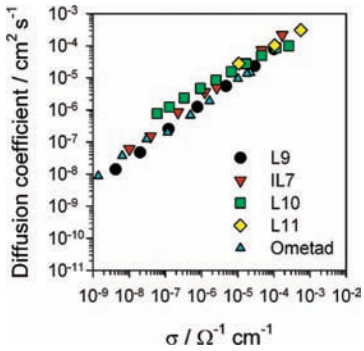

Figure 5. Diffusion coefficient in several DSCs as a function of electron conductivity.

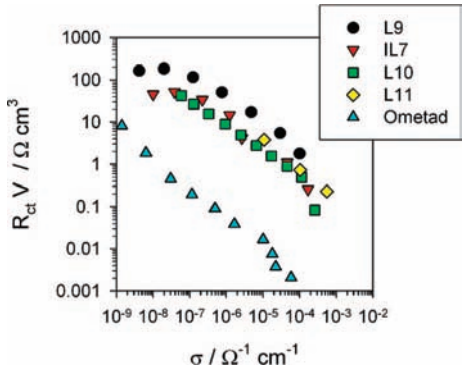

Figure 6. Recombination resistance normalized to volume in several DSCs as a function of electron conductivity.

The chemical capacitances[23,24] of TiO_2 in different DSCs (Figure 4) present a small variation in their slopes depending on the sample. This is an indication of small differences in the tail distribution of electrons below the conduction band that may be attributed to the use of different dyes, TiO_2 paste series and hole transporter media, and their additives. It appears from Figure 4 that the higher slope we obtain, i.e., higher α parameter in $C_\mu = C_0 \exp[-\alpha(E_{cb} - E_{Fn})/k_BT]$ (here $0.2 < \alpha < 0.4$), the better efficiency can be obtained.

With transport resistance, R_t, and the chemical capacitance, C_μ, of TiO_2 obtained from impedance, it is possible to calculate the chemical diffusion coefficient, D_n, with the expression[19]

$$D_n = \frac{L^2}{R_t C_\mu} \qquad (2)$$

L being the total thickness of the film. The evolution of the chemical diffusion coefficient in spiro-OMeTAD (Figure 5) indicates that there are no variations in the transport characteristics of electrons in TiO_2, once the same conductivity level is reached. The observed trend for the chemical diffusion coefficient is described in previous works,[13,19] i.e., D_n increases when the Fermi level is raised. Therefore, we can conclude that once the same position of the Fermi level with respect to the conduction band is reached, electron transport is not influenced by the DSC configuration. This is, in our view, a very important result that leads us to focus our attention on recombination characteristics for interpreting the different performances observed according to the hole transport medium.

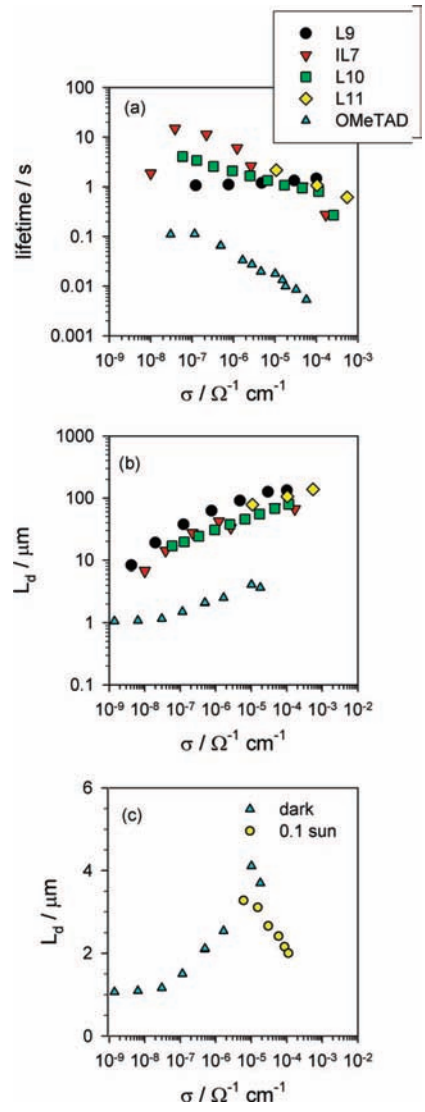

Figure 7. Recombination time (a) and effective diffusion length (b) in several DSCs as a function of electron conductivity. (c) Effective diffusion length of spiro-OMeTAD shown ion a linear scale both in the dark and under illumination.

Considering the recombination resistance shown in Figure 6, we observe that the recombination rate is 2 orders of magnitude larger in the spiro-OMeTAD SDSC, for the same occupancy of the TiO_2 conduction band, than in the other cells. This result is in close agreement with the recombination kinetics being 100 times faster in spiro-OMeTAD than in liquid electrolyte, as obtained before by transient absorption spectroscopy.[25] Thus, recombination becomes the major feature determining the lower efficiency of the solid cell.

Some shunt from the back layer is observed at the short circuit region of the $j-V$ curve (Figure 1a) at high illumination conditions, while this is not observed at low light intensity. In this region, most of the recombination is produced in the blocking underlayer zone of the SDSC. However, at higher operating potentials and, in particular, at peak power potential, all the TiO_2 film is contributing to recombination. The total recombination surface is the sum of the flat 100 nm thick blocking layer, plus the 20 nm diameter TiO_2 nanocolloids

(23) Bisquert, J. *Phys. Chem. Chem. Phys.* **2003**, *5*, 5360.
(24) Bisquert, J.; Fabregat-Santiago, F.; Mora-Seró, I.; Garcia-Belmonte, G.; Barea, E. M.; Palomares, E. *Inorg. Chim. Acta* **2008**, *361*, 684–698.
(25) Hirata, N.; Kroeze, J. E.; Park, T.; Jones, D.; Haque, S. A.; Holmes, A. B.; Durrant, J. R. *Chem. Commun.* **2006**, 535–537.

surface, the latter being more than 100 times larger than the former. Therefore, we have assumed that recombination occurs mainly in the mesoporous TiO_2 film.

It was shown in Figure 3 that the spiro-OMeTAD SDSC could, in principle, reach higher photovoltage than the other cells, due to a lower position of the hole Fermi level. However, it can be seen in Table 1 that such higher V_{oc} is not realized. This is explained by the intense recombination that is apparent in the lower values of R_{ct} in the SDSC. In addition, the low R_{ct} is the key factor in the low values found for both the recombination time of electrons in TiO_2 ($\tau_n = R_{ct}C_\mu$) and its effective diffusion length [$L_n = (R_{ct}/R_t)^{1/2} = (D_n\tau)^{1/2}$] (Figure 7).

Therefore, recombination time in spiro-OMeTAD sample is almost 2 orders of magnitude larger than in the liquid cells, as previously found in several studies[2,7,8,25−27] (Figure 7a). A similar result is found for the effective diffusion length (Figure 7b). The short L_n does not allow the use of thick TiO_2 layers in OMeTAD cells,[3] limiting the available surface for dye loading and, therefore, light absorption and current injection. It has to be noted that the effective diffusion length obtained here is lower than the diffusion length of electrons in the conduction band as measured by IMPS by Peter et al. and Snaith et al. in their recent works.[7,9] However, our results suggest that the effective diffusion length is controlling the behavior of the cells, at least at potentials where the full nanostructured layer is active, which includes potentials near peak power and above.

The results shown in Figure 7b for SDSC, in which L_n grows when increasing the position of the Fermi level in TiO_2, apparently contradict those found previously in other works.[7,8] However, it has to be taken into account that our measurements are made in the dark, and they present a maximum value near the higher conductivities measured; it was not possible to extend further these measurements. When we illuminate the samples (Figure 7c), the effective diffusion length drops when increasing the conductivity in TiO_2. A more detailed study of the behavior of L_n is out of the scope of this work, but it appears interesting to further explore by impedance spectroscopy the variations of the diffusion length in the presence of photogenerated holes,[7,8] and this will be attempted in the future.

The limit of current injection due to the small thickness of the cell, added to the problem of charge collection due to losses by recombination, implies that although the distance between E_{cb} and E_{Fp} in the SDSC is larger than in the other DSCs (Figure 2), the efficiency may not be as large at any circumstance. Thus, both interfacial blocking treatments and the use of higher extinction coefficient dyes are needed to improve SDSC performance.

Finally we analyze the values obtained for the resistance in the spiro-OMeTAD (Figure 8). The first important feature is

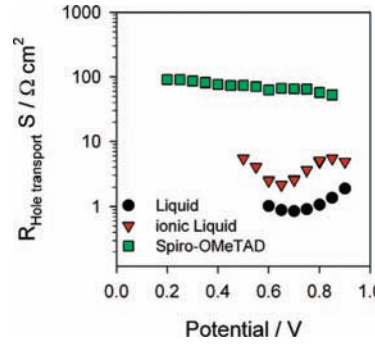

Figure 8. Normalized hole transport resistance in spiro-OMeTAD, liquid, and ionic liquid DSCs under illumination. The normalization was done following $R_{hole\ transport}S = (\rho L)pf$, with $R_{hole\ transport}$ the resistance of the hole conductor, calculated from impedance, S the active surface of the sample, ρ the resistivity, L the thickness of the hole conductor layer (the same as the sample thickness), and pf the pore filling level.

that R_{OMeTAD} presents very slight variations over the range of potentials measured (and within the precision of the fit). This fact confirms our initial supposition that the Fermi level of holes in the spiro-OMeTAD is stationary under bias voltage variation.

The second relevant feature is the large value of R_{OMeTAD}, at least one 1 order of magnitude higher than those obtained with the other (electrolytic) hole transport media (Figure 8).[14] It has to be noted that, for potentials higher than 0.65 V, the resistance for hole transport in the OMeTAD becomes larger than the resistance for electron transport in the TiO_2. As a consequence, the SDSC has a large contribution to the series resistance of the cell due to R_{OMeTAD}, and this produces a much poorer fill factor on the cell response. This situation will become worse if current injection is increased. Therefore, stronger doping of spiro-OMeTAD is needed to overcome this problem, taking care not to increase the optical absorbance in the visible region,[28] in order to maintain large rates of charge generation.

Conclusions

We have shown that mechanisms of transport of electrons in the TiO_2 in DSCs in the dark remain unaltered, independent of the hole transporter media used. The main limitation in the solar cell is attributed to the high transfer rate at the interface between TiO_2 and spiro-OMeTAD, which limits the diffusion length and recombination time of the SDSC. Furthermore, the origin of the low fill factor found in the solid DSC has been attributed to the high transport resistance in the spiro-OMeTAD.

Acknowledgment. This work has been supported by the European Science Foundation and Ministerio de Ciencia e Innovación under project 05-SONS-FP-021 (MAT2006-28187-E), the MICINN under project HOPE CSD2007-00007 (Consolider-Ingenio 2010), and the Generalitat Valenciana under projects GV06/347 and BEST/2007/015. P.C. thanks the Taiwan Merit Scholarships Program, TMS-094-2A-026, for financial support.

JA805850Q

(26) Fabregat-Santiago, F.; García-Cañadas, J.; Palomares, E.; Clifford, J. N.; Haque, S. A.; Durrant, J. R.; Garcia-Belmonte, G.; Bisquert, J. *J. Appl. Phys.* **2004**, *96*, 6903.

(27) Handa, S.; Wietasch, H.; Thelakkat, M.; Durrant, J. R.; Haque, S. A. *Chem. Commun.* **2007**, 1725.

(28) Snaith, H. J.; Grätzel, M. *Appl. Phys. Lett.* **2006**, *89*, 262114.